

Spin Polarization Inversion at Benzene-Absorbed Fe₄N Surface

Qian Zhang¹, Wenbo Mi^{1,*}, Xiaocha Wang², and Xuhui Wang^{3,*}

¹*Tianjin Key Laboratory of Low Dimensional Materials Physics and Preparation Technology, Faculty of Science, Tianjin University, Tianjin 300072, China*

²*Tianjin Key Laboratory of Film Electronic & Communicate Devices, School of Electronics Information Engineering, Tianjin University of Technology, Tianjin 300384, China*

³*Physical Science and Engineering Division, King Abdullah University of Science and Technology (KAUST), Thuwal 23955-6900, Kingdom of Saudi Arabia*

* Author to whom all correspondence should be addressed.

E-mail: miwenbo@tju.edu.cn and xuhuiwangnl@gmail.com

ABSTRACT

We report a first-principle study on electronic structure and simulation of the spin-polarized scanning tunneling microscopy graphic of a benzene/Fe₄N interface. Fe₄N is a compound ferromagnet suitable for many spintronic applications. We found that, depending on the particular termination schemes and interface configurations, the spin polarization on the benzene surface shows a rich variety of properties ranging from cosine-type oscillation to polarization inversion. Spin-polarization inversion above benzene is resulting from the hybridizations between C p_z and the out-of-plane d orbitals of Fe atom.

Keywords: Spin-polarization inversion, Absorption, Interfaces

PACS: 72.25.-b, 68.43.Bc, 73.20.-r

Introduction

In recent years, combining inorganic and organic materials have opened many venues for the novel science and applications. The rising field of organic spintronics is one of them¹⁻⁶. Organic materials, with long spin-flip diffusion length and weak spin-orbit coupling, are desirable in many spintronic applications^{2, 7-17}. Moreover, the functionalities of devices made of organic materials can be manipulated through relatively simple methods such as ligand modification^{18, 19} and isomerization^{20, 21}.

A major topic in organic spintronics is the spin related properties at the interface between a ferromagnetic substrate and organic material, i.e. the spinterface²². Much effort has been made to clarify the underlying mechanisms that drive the peculiarities, such as spin polarization inversion, at various spinterfaces^{21, 23-26}. For the interfaces between Fe and benzene molecule (as well as C₅H₅ and C₈H₈), Atodiresei *et al.* argue that it is the p_z - d Zener exchange-type mechanism that leads to the spin-polarization inversion²⁴. In another study on the thiophene/cobalt(001) interface²⁵, the strong spatial dependence of the spin polarization at the interface is attributed to the reduced molecular symmetry. The azobenzene isomer adsorbed on Fe surface has been reported recently, where the switch between two types of azobenzenes takes place by applying light and/or heat²¹. On the other hand, studies are extended to systems consisting of AFM substrates including benzene adsorbed on monolayer AFM Mn²⁶ or metal

phthalocyanine^{4, 27-29}, where the spin polarization modification has often been reported.

But, we are not aware of any investigations into the interfaces between an organic molecule and a compound ferromagnet, such as iron nitride (Fe_4N). Fe_4N carries a high spin polarization of nearly $\sim 100\%$ ³⁰ as well as a large saturation magnetization of 1200 emu/cm^3 ³¹. Its Curie temperature is about 760 K. Together with its high chemical stability³² and low coercivity³³, Fe_4N is a promising candidate for, among other, spin injection source³⁴. In this work, we scrutinize the spinterface between a benzene molecule and Fe_4N substrate. In particular, we will show that different termination schemes and adsorption configurations unique to the benzene/ Fe_4N interface enrich the properties of spin polarization.

Calculation details

Our first principles calculations are based on the density-functional theory (DFT) and the projector augmented wave method as implemented in the Vienna Ab initio Simulation Package code^{35, 36}. For the exchange and correlation functional, we use the Perdew-Burke-Ernzerhof spin-polarized generalized gradient approximation (PBE-GGA)³⁷. The plane-wave basis set is converged using a 500 eV energy cutoff. A Γ -centered $3\times 3\times 1$ k -mesh is used for the Brillouin-zone integrations. A Gaussian smearing of 0.02 eV is used for the initial occupations. It is worth pointing out that van

der Waals force is excluded from our calculation. We do so not only because strong bonding exists between benzene molecule and Fe₄N (as shown in the due discussion), but also recent studies suggest that it has a negligible effect on GGA optimized structure in, for example, azobenzene/Fe(110)²¹.

Bulk Fe₄N has a cubic perovskite-type structure (*Pm3m*) with a lattice constant of 3.795 Å³⁴. Fe occupies the corner (Fe_I) or face-centered (Fe_{II}) position labeled structure graphic of bulk Fe₄N, whereas N locates at the body-centered site³⁴, as shown in Fig. 1(a). Our calculations give a lattice constant of 3.789 Å, in agreement with the experimental value³⁴. The Fe₄N substrate is modeled by slabs of three atomic layers with a (3×3) flat surface. We concentrate, in this work, on the effect of different adsorption schemes on the spatial spin-polarization distribution. The subtleties due to the number of atomic layers will be reported in upcoming studies.

Termination schemes and interface models

The benzene/Fe₄N interfaces are modeled by placing benzene on top of the Fe₄N(001) surface. The lattice structure of Fe₄N allows us to have the interfaces with two types of terminations, namely, Fe_{II}N and Fe_IFe_{II}. For Fe_{II}N termination, Fe₄N surface is the plane across the body-centered site parallel to Fe₄N(001). For Fe_IFe_{II} termination, Fe₄N surface refers to the plane across the face-centered site. For each

termination scheme, we further consider two stacking models based on whether N or Fe atom, in the first layer, is right beneath the center of benzene molecule: models $\text{Fe}_{\text{II}}\text{N-C}$ and $\text{Fe}_{\text{I}}\text{Fe}_{\text{II}}\text{-C}$ are named after the terminations with N or Fe atom in the Fe_4N surface, locating right beneath the center of benzene molecule, whereas models $\text{Fe}_{\text{II}}\text{N-NC}$ and $\text{Fe}_{\text{I}}\text{Fe}_{\text{II}}\text{-NC}$ are referring to the ones without, see Fig. 1. During the lattice structure relaxation, the atoms in the bottom layer of slab are fixed at their bulk positions, whereas other atoms are fully relaxed until the force is weaker than 0.03 eV/Å. In order to decouple adjacent slabs, a thick vacuum layer of 15 Å is included in the direction perpendicular to the surface. To illustrate the nature of the spin-polarization inversion in the real space, we calculate the spin-polarization distribution by the constant-height spin-polarized scanning tunneling microscopy (SP-STM) simulation³⁸.

Results and discussion

To illustrate the system, we also define the surface (inter layer, fixed layer) of Fe_4N slab as I (II, III) layer, and the benzene as M layer. We call the zone above benzene as ‘benzene surface’, between benzene and Fe_4N as ‘interfaces’, and atoms of I layer, in Fe_4N slab, as ‘ Fe_4N surface’. The sites where the Fe ion located right below the C atom are defined as the top ($_t$) sites; the ones where the Fe ion located under the

C-C bond are defined as the bridge ($_b$) sites. At the top or bridge sites, we call the Fe (C) atom by Fe $_t$ (C $_t$) or Fe $_b$ (C $_b$). The atom located right under the center of benzene is Fe $_c$ or N $_c$. Figures 1(c), (d), (e) and (f) show the side and top views of the four optimized stacking models. After the structure relaxation, benzene plane is no longer flat in all models except Fe $_{II}$ N-NC. Especially, the hydrogen atoms in Fe $_{II}$ N-C and Fe $_I$ Fe $_{II}$ -NC models lie fairly further away from the slab surface than carbon atoms, agreeing with earlier reports^{18, 24}. The C-C bonds become longer than those in the isolated benzene ring.

The Fe $_4$ N slab also experiences the structural changes. In both Fe $_{II}$ N-C and Fe $_I$ Fe $_{II}$ -NC models, the Fe $_t$ and Fe $_b$ atoms move out of the Fe plane of the surface, see Fig. 1(c) and (f). In the Fe $_I$ Fe $_{II}$ -C model, Fe $_c$ moves up, as shown in Fig. 1(e). In the exception arises from the Fe $_{II}$ N-NC model, where the benzene plane is still flat, yet the C-C bonds are equal to that in the isolated benzene. The benzene plane is moving away from the Fe $_4$ N surface, as shown in Fig. 1(d). The data from our calculation is in the Table 1.

The adsorption energy (E_{abs}) of different models is labeled in Fig. 1(b). According to the adsorption energy, 4 adsorption models fall into two categories: the endothermic adsorption (two Fe $_{II}$ N terminals models) and exothermic adsorption (two Fe $_I$ Fe $_{II}$ terminals models). The Fe $_{II}$ N-C model has the maximum adsorption energy (0.74 eV). This implies that, at high temperatures, it is the most easily formed model among the

four. On the other hand, Fe_IFe_{II}-NC shows an exothermic adsorption with the minimum adsorption energy (-2.14 eV), implying that its stability favours low temperatures.

The moment and charge are listed in Table 2. The charge value is calculated using Bader analysis³⁹⁻⁴¹. We note that the Fe_{II} moment in layer II, see the 3rd row in Table 2, is smaller than 2.29 μ_B in bulk Fe₄N, where μ_B is Bohr magneton. This is due to a stronger yet more localized hybridization between N and Fe_{II} in the second layer⁴²⁻⁴⁴. Apart from the exception in the Fe_{II} ions in layer II, in Fe_IFe_{II} terminal, we observe that, while it gains more charge, the Fe_{II} moment tends to be larger than that in bulk Fe₄N. But in the Fe_{II}N terminal, this relation no longer holds; no prominent relationship between charge and moment is present.

To understand the bonding mechanisms, we analyze the charge density difference defined by $\Delta\rho = \rho_{C_6C_6/Fe_4N} - \rho_{C_6H_6} - \rho_{Fe_4N}$, where $\rho_{C_6C_6/Fe_4N}$, $\rho_{C_6H_6}$ and ρ_{Fe_4N} are the charge densities of the full system, isolated benzene and Fe₄N surface, respectively. Charge accumulation (depletion) is in yellow (blue). In the Fe_{II}N-C model, the charge accumulates on the C-Fe bonds, as Fig. 2(a) shows. In Fig. 2(b), the interface has little charge accumulation between C and Fe ions, indicating that C atoms do not form bonds with Fe₄N slab. This is consistent with the large distance between the benzene and Fe₄N surface. Figure 2(c) displays a large charge accumulation in the region right below benzene in the Fe_IFe_{II}-C model. In the Fe_IFe_{II}-NC model, the charge depletion distributes around the centerline perpendicular to Fe₄N surface, and significant charge

accumulation appears around the C_t-Fe_t and C_b-Fe_b bonds, as shown in Fig. 2(d).

The C atom captures only approximately $0.1\sim 0.2|e|$, suggesting the covalent characteristics of the C-Fe bonds.

A general picture of bonding mechanism between the benzene and different Fe₄N terminations can be further extracted from the spin-resolved density-of-states (DOS), as Figs. 3 and 4 show. The 3d orbitals can be divided into two classes according to the symmetry: the out-of-plane orbitals (d_{z^2} , $d_{xz}+d_{yz}$) and the in-plane ones ($d_{xy}+d_{x^2-y^2}$). In the Fe_{II}N-C model, for the top sites, Fe_t d_{z^2} and $d_{xz}+d_{yz}$ hybridize with C_t p_z in the energy interval of -4.25~-3.5 eV for both the spin-up and spin-down states. At about 2.79 eV, the hybridization is just for the spin down states. Meanwhile, the Fe_t spin-up d_{z^2} has hybridization with C_t p_z at 1.80 eV.

For the bridge sites, we note that the spin-up and spin-down π orbitals of benzene are mixed with Fe_b d_{z^2} and $d_{xz}+d_{yz}$ in -4.14~-3.5 eV energy interval, and with Fe_b spin-down $d_{xz}+d_{yz}$ at 2.54 eV. Besides the strong hybridization that mentioned above, a series of hybridizations between the C p_z and Fe d states are drawn in Fig. 3(a). For Fe at both the top and bridge sites, its s and d orbitals, for both spin species, hybridize with the N_c p orbitals in the energy interval -7.6~-3.8 eV. The degenerated p_x+p_y orbitals of N_c hybridize with Fe $d_{xy}+d_{x^2-y^2}$ in the energy interval 2.0~5.0 eV. And this hybridization between the spin-down p_z of C and d_{z^2} , $d_{xy}+d_{x^2-y^2}$ of Fe_t and Fe_b is fairly strong at -0.43 eV.

In Fig. 3(b) for the Fe_{II}N-NC model, the benzene π orbitals originating from the C p_z orbitals do not hybridize with Fe. The slab keeps mostly the properties of a clean surface. The N p_x and p_y orbitals are degenerate. The DOS of Fe_t is almost the same as that of Fe_b. Meanwhile, the Fe_{II} $d_{xz}+d_{yz}$ orbitals hybridize with the N p_z orbitals in the energy interval -4.1~-6.6 eV and at Fermi energy (E_F). The Fe_{II} $d_{xy}+d_{x^2-y^2}$ and s orbitals are mixed with the degenerate N p_x, p_y orbitals at -6.6~-7.2 eV.

In the Fe_IFe_{II} terminations, the intensity of local benzene π orbitals peak become weak gradually, and the peak becomes wider. Figure 4 shows the DOS of two Fe_IFe_{II} terminations. In the Fe_IFe_{II}-C model, Fe_c $d_{xz}+d_{yz}$ hybridizes with C p_z at -5.1 eV, and with C p_x, p_y at -7.9 eV, as shown in Fig. 4(a). The Fe_c d_{z^2} orbitals hybridize with C p_z in the energy interval -6.7~-6.3 eV. The hybridization between the Fe_c spin-up $d_{xy}+d_{x^2-y^2}$ and C p_z is strengthened in the energy interval of 1.1~2.1 eV. At the energy level above 2.5 eV, Fe_c spin-down d_{z^2} weakly hybridizes with C_t p_z .

In the Fe_IFe_{II}-NC model, we see a rather weak mixture between the C_t p_z and Fe_t $d_{z^2}, d_{xz}+d_{yz}$ states in the interval -7.4~-6.0 eV. We note that C_t p_z orbitals tend to degenerate with the p_x orbitals, yet C_b shows no such tendency. In the interval -5.5~-4.0 eV, the prime conjugate peaks consist of Fe_b s and C_b p_z orbitals. At -1.75 eV, the Fe_b spin-down $d_{xz}+d_{yz}$ and $d_{xy}+d_{x^2-y^2}$ have hybridization with the C_b p_z orbitals.

We note a trend from the above hybridization schemes. As the benzene molecule

moves towards the Fe₄N surface, the hybridization of different orbitals depends on the termination schemes. In the Fe_{II}N-C and Fe_IFe_{II}-C models, the Fe $d_{xz}+d_{yz}$ and d_{z^2} orbitals hybridize strongly with the C p_z state, leading to spin-polarization inversion. In the Fe_IFe_{II}-NC model, the hybridization between both spin species of the C p_z and Fe s , $d_{xy}+d_{x^2-y^2}$ orbitals is stronger than that between C p_z and Fe ($d_{xz}+d_{yz}$, d_{z^2}), unable to reverse the spin polarization. This is consistent with the report in Ref. 17. We are thus led to conclude that the spin-polarization inversion at benzene surface is a result of hybridizations between the p_z orbital of C and the out-of-plane Fe d orbitals.

We show, in Fig. 5, the spatial distribution of spin-polarization P_{space} , defined as

$$P_{space} = \frac{n_s^{\uparrow}(\mathbf{r}_{\square}, z, \varepsilon) - n_s^{\downarrow}(\mathbf{r}_{\square}, z, \varepsilon)}{n_s^{\uparrow}(\mathbf{r}_{\square}, z, \varepsilon) + n_s^{\downarrow}(\mathbf{r}_{\square}, z, \varepsilon)}, \quad (1)$$

for an energy interval of $[\varepsilon, E_F]$. $n_s^{\uparrow\downarrow}(\mathbf{r}_{\square}, z, \varepsilon)$ is the spin-up (down) charge density in real space, at position \mathbf{r}_{\square} and a distance z from the surface. Here, the value of ε is either $E_F-0.4$ eV or $E_F+0.4$ eV^{21, 28}. In this figure, we focus on two energy intervals, $[E_F-0.4$ eV, $E_F]$ and $[E_F, E_F+0.4$ eV]. In each energy interval, the spin-polarization is projected onto the plane that is parallel to the Fe₄N surface, see Figs. 5(b) and (c); the distance between the plane and benzene surface is labeled in Fig. 5(b). For the 4 models discussed in this work, we plot, in Figs. 5(a) and (d), the spin polarization

along a few selected lines defined in Figs. 5(b) and (c).

For the Fe_{II}N-C model, the highest spin polarization is ~80%, and the lowest value is ~-60% via line 2 and line 3, see Fig. 5(a). The intensity of inversion is much stronger than benzene adsorbed antiferromagnetic Mn²⁶, due to the hybridization between the p_z states and d_{z^2} , d_{xy} + $d_{x^2-y^2}$ orbitals of Fe_t and Fe_b at -0.43 eV. This hybridization enhances the population of the spin-down species, and is thus reversing the spin polarization. It is interesting to note that the spin-polarization distributions in the energy interval $[E_F-0.4 \text{ eV}, E_F]$ and $[E_F, E_F+0.4 \text{ eV}]$ are rather different, even with opposite signs. This suggests that the sign of spin polarization can be reversed by simply shifting the E_F by, for example, applying a gate voltage.

In the Fe_{II}N-NC model, line 2 exhibits the spin-polarization inversion, as shown in Fig. 5(b). The DOS, in Fig. 3(b), however, points to a weak adsorption. The spin-polarization distribution in this model is thus similar to that in vacuum (above a clean Fe₄N surface). For the Fe_{II}N-NC model, the spin polarization of line 1 with a cosine-type distribution is shown in Fig. 5(a).

In both Fe_IFe_{II} terminal models, spin-polarization inversion happens, but the strong spin-polarization inversion in the neighbourhood of benzene happens only in Fe_IFe_{II}-C. In Fe_IFe_{II} terminations, Fe₄N surface distort significantly, Fe_{II} ions are not located right above N atoms, as shown in Figs. 1(e) and (f). Then positive spin polarization of N atoms extends into benzene surface. In Fe_IFe_{II}-C model, the most

interesting feature is that the positive spin-polarization distributes along the C-C bonds, see Fig. 5(b). In Fig. 6, a positive spin polarization of benzene appears at E_F in the $\text{Fe}_I\text{Fe}_{II}\text{-C}$ model. On the other hand, in the $\text{Fe}_I\text{Fe}_{II}\text{-NC}$ model spin polarization is approximate 0%. Meanwhile spatial spin-polarization, for $\text{Fe}_I\text{Fe}_{II}\text{-NC}$, in the neighbourhood of benzene is almost 0%, see Fig. 5(b). So, the atomic scale spin-polarization, at benzene surface, is modulated by N and C atoms.

Figure 7 is the spin-polarization plane of $\text{Fe}_{II}\text{N-C}$ structure. It's across the top sites and parallel to $\text{Fe}_4\text{N}(100)$. From this figure, benzene hampers the extension of N position spin polarization, and realizes the spatial spin polarization inversion. The reason is the overlap of p_z and out-of-plane components of d .

Conclusion

In summary, we have shown that at the spinterface formed by benzene adsorbed on Fe_4N , depending on the specific termination schemes, a variety of spin polarization, including spin polarization inversion, can take place. The spin-polarization inversion finds its origin in the hybridization between the out-of-plane components of Fe d orbitals and the benzene π orbitals (the p_z orbital, in particular). The presence of N atoms partition the adsorption into two categories: the endothermic (adsorption) Fe_{II}N terminal models and the exothermic $\text{Fe}_I\text{Fe}_{II}$ terminal ones. With these results, we can

see that adsorptions rely on the temperature. The $\text{Fe}_{11}\text{N-C}$ with the maximum adsorption energy will be easier to be formed than others under high temperature and has significant spin-polarization inversion, which is desired for the spintronic devices.

Acknowledgements

This work is supported by the National Natural Science Foundation of China (51171126), Key Project of Natural Science Foundation of Tianjin City (12JCZDJC27100 and 14JCZDJC37800), Program for New Century Excellent Talents in University (NCET-13-0409), Scientific Research Foundation for the Returned Overseas Chinese Scholars, State Education Ministry. It is also supported by High Performance Computing Center of Tianjin University, China.

References

1. Xiong, Z. H., Wu, D. Z., Vardeny, V. & Shi, J. Giant magnetoresistance in organic spin-valves. *Nature* **427**, 821-824 (2004).
2. Dediu, V., Murgia, M., Maticcotta, F. C., Taliani, C. & Barbanera, S. Room temperature spin polarized injection in organic semiconductor. *Solid State Commun.* **122**, 181-184 (2002).
3. Drew, A. J. *et al.* Direct measurement of the electronic spin diffusion length in a fully functional organic spin valve by low-energy muon spin rotation. *Nat. Mater.* **23**, 109-114 (2008).
4. Mugarza, A. *et al.* Electronic and magnetic properties of molecule-metal interface: Transition-metal phthalocyanines adsorbed on Ag(100). *Phys. Rev. B* **85**, 155437 (2012).
5. Rybicki, J. *et al.* Tuning the performance of organic spintronic devices using X-Ray generated traps. *Phys. Rev. Lett.* **109**, 076603 (2012).
6. Sun, D. *et al.* Giant magnetoresistance in organic spin valves. *Phys. Rev. Lett.* **104**, 236602 (2010).
7. Dediu, V., Hueso, L. E., Bergenti, I. & Taliani, C. Spin routes in organic semiconductors. *Nature Mater.* **8**, 707-716 (2009).
8. Xu, W. *et al.* Tunneling magnetoresistance observed in $\text{La}_{0.67}\text{Sr}_{0.33}\text{MnO}_3$ /organic

- molecule/Co junctions. *Appl. Phys. Lett.* **90**, 072506 (2007).
9. Vinzelberg, H. *et al.* Low temperature tunneling magnetoresistance on (La, Sr)MnO₃/Co junctions with organic spacer layers. *Appl. Phys. Lett.* **103**, 093720 (2008).
 10. Dediu, V. *et al.* Room-temperature spintronic effects in Alq₃-based hybrid devices. *Phys. Rev. B* **78**, 115203 (2008).
 11. Barraud, C. *et al.* Unravelling the role of the interface for spin injection into organic semiconductors. *Nat. Phys.* **6**, 615-620 (2010).
 12. Steil, S. *et al.* Spin-dependent trapping of electrons at spinterfaces. *Nat. Phys.* **9**, 242-247 (2013).
 13. Dediu, V. A. Organic spintronics: Inside the interface. *Nat. Phys.* **9**, 210-211 (2013).
 14. Santos, T. S. *et al.* Room-temperature tunnel magnetoresistance and spin-polarized tunneling through an organic semiconductor barrier. *Phys. Rev. Lett.* **98**, 016601 (2007).
 15. Jiang, J.S., Pearson, J.E. & Bader, S. D. Absence of spin transport in the organic semiconductor Alq₃. *Phys. Rev. B* **77**, 035303 (2008).
 16. Davis, A. H. & Bussmann, K. Organic luminescent devices and magnetoelectronics. *J. Appl. Phys.* **93**, 7358-7360 (2003).
 17. Rocha, A. R. *et al.* Towards molecular spintronics. *Nat. Mater.* **4**, 335-339 (2005).

18. Atodiresei, N., Caciuc, V., Lazić, P. & Blügel, S. Engineering the magnetic properties of hybrid organic-ferromagnetic interfaces by molecular chemical functionalization. *Phys. Rev. B* **84**, 172402 (2011).
19. Friedrich, R. *et al.* Electronic states and the influence of oxygen addition on the optical absorption behaviour of manganese phthalocyanine. *J. Chem. Phys.* **136**, 064704 (2012).
20. Friedrich, R., Kersting, B. & Kortus, J. Fermi level engineering in organic semiconductors for controlled manufacturing of charge and spin transfer materials. *Phys. Rev. B* **88**, 155327 (2013).
21. Wang, Y., Che, J. G., Fry, J. N. & Cheng, H. P. Reversible spin polarization at hybrid organic-Ferromagnetic interfaces. *J. Phys. Chem. Lett.* **4**, 3508-3512 (2013).
22. Sanvito, S. Molecular spintronics: The rise of spinterface science. *Nat. Phys.* **6**, 562-564 (2010).
23. Qi, S. F., Ning, W. W. & Xu, X. H. The spin-filter role of the ill-defined layer in FM/Alq₃/FM organic spin valve: A first-principle study. *Synth. Met.* **177**, 82-88 (2013).
24. Atodiresei, N. *et al.* Design of local spin polarization at the organic-ferromagnetic interface. *Phys. Rev. Lett.* **105**, 066601 (2010).
25. Wang, X., Zhu, Z., Manchon, A. & Schwingenschlögl, U. Peculiarities of spin polarization inversion at a thiophene/cobalt interface. *Appl. Phys. Lett.* **102**,

111604 (2013).

26. Caffrey, N. M., Ferriani, P., Marocchi, S. & Heinze, S. Atomic-scale inversion of spin polarization at an organic-antiferromagnetic interface. *Phys. Rev. B* **88**, 155403 (2013).
27. Sun, X., Wang, B. & Yamauchi, Y. Electronic structure and spin polarization of metal (Mn, Fe, Cu) phthalocyanines on an Fe(100) surface by first-principles calculations. *J. Phys. Chem.* **116**, 18752-18758 (2012).
28. Amin, B., Nazir, S. & Schwingenschlögl, U. Molecular distortion and charge transfer effects in ZnPc/Cu(111) *Sci. Rep.* **3**, 1705 (2013).
29. Sun, X., Wang, B., Pratt, A. & Yamauchi, Y. Magnetic moment enhancement and spin polarization switch of the manganese phthalocyanine molecule on an IrMn(100) surface. *J. Chem. Phys.* **141**, 034703 (2014).
30. Jang, Y. R., Kim, I. G. & Lee, J. I. Electronic structure and magnetic properties of Fe₄N(001). *J. Magn. Magn. Mater.* **263**, 366-372 (2003).
31. Shirane, G., Takei, W. J. & Ruby, S. L. Mössbauer study of hyperfine fields and isomer shifts in Fe₄N and (Fe, Ni)₄N. *Phys. Rev.* **126**, 49 (1962).
32. Lee, T. H. D., Hu, S. & Madulid, N. Stability studies of iron particle. *IEEE Trans. Magn.* **23**, 2880-2882 (1987).
33. Tagawa, K., Kita, E. & Tasaki, A. Synthesis of fine Fe₄N powder and its magnetic characteristics. *Jpn. J. Appl. Phys.* **21**, 1596-1598 (1982).

34. Mi, W. B., Guo, Z. B., Feng, X. P. & Bai, H. L. Reactively sputtered epitaxial γ -Fe₄N films: Surface morphology, microstructure, magnetic and electrical transport properties. *Acta Mater.* **61**, 6387-6395 (2013).
35. Kresse, G. & Furthmüller, J. Efficient iterative schemes for ab initio total-energy calculations using a plane-wave basis set. *Phys. Rev. B* **54**, 11169 (1996).
36. Kresse, G. & Joubert, D. From ultrasoft pseudopotentials to the projector augmented-wave method. *Phys. Rev. B* **59**, 1758 (1999).
37. Perdew, J. P., Burke, K. & Ernzerhof, M. Generalized gradient approximation made simple. *Phys. Rev. Lett.* **77**, 3865 (1996).
38. Wortmann, D., Heinze, S., Kurz, Ph., Bihlmayer, G. & Blügel, S. Resolving complex atomic-scale spin structures by spin-polarized scanning tunneling microscopy. *Phys. Rev. Lett.* **86**, 4132 (2001).
39. Henkelman, G., Arnaldsson, A. & Jónsson, H. A fast and robust algorithm for Bader decomposition of charge density. *Comput. Mater. Sci.* **36**, 354-360 (2006).
40. Sanville, E., Kenny, S. D., Smith, R. & Henkelman, G. Improved grid-based algorithm for bader charge allocation. *J. Comput. Chem.* **28**, 899-908 (2007).
41. Tang, W., Sanville, E. & Henkelman, G. A grid-based bader analysis algorithm without lattice bias. *J. Phys.: Condens. Matter* **21**, 084204 (2009).
42. Dunn, J. H., Arvanitis, D. & Martensson, N. Magnetism of thin Fe films on Cu(100). *Phys. Rev. B* **54**, R11157 (1996).

43. Nakagawa, T., Takagi, Y., Matsumoto, Y. & Yokoyama, T. Enhancements of spin and orbital magnetic moments of submonolayer Co on Cu(001) studied by X-ray magnetic circular dichroism using superconducting magnet and liquid He cryostat. *Jpn. J. Appl. Phys.* **47**, 2132-2136 (2008).
44. Shi, Y. J., Du, Y. L. & Chen, G. Ab initio study of structure and magnetic properties of cubic Fe₄N(001) surface. *Solid State Commun.* **152**, 1581-1584 (2012).

Author contributions

All authors designed the outline of the manuscript. Q.Z. and W.B.M. wrote the main text; X.C.W. and X.H.W. contributed detailed discussions and revisions; All authors reviewed the manuscript.

Competing financial interests statement

Competing financial interests:

The authors declare no competing financial interests.

Table notes

Table 1. Special bonds of different adsorbed structures comparing to the clear Fe₄N surface. The bonds of isolated benzene is 1.398 Å. X-up-Y means that the average vertical distance between X and Y plane. When Y=Fe, Y stands for the Fe atoms in layer I.

Bond (Å)	Adsorbed				Clear	
	Fe _{II} N-C	Fe _{II} N-NC	Fe _I Fe _{II} -C	Fe _I Fe _{II} -NC	Fe _{II} N	Fe _I Fe _{II}
IL-III	1.674	1.636	1.772	1.834	1.701	1.706
III-III	1.836	1.813	1.897	1.872	1.754	1.844
N-up-Fe	0.292	0.344	-	-	0.343	(Fe)0.200
M-IL	2.353	3.634	1.997	1.983	-	-
C _t -C _b	1.442	1.398	1.418	1.442	-	-
C _b -C _b	1.408	1.399	1.437	1.463	-	-
H-up-C	0.266	0	0.098	0.360	-	-
Fe _t -up-Fe	0.319	0	-	0.139	-	-
Fe _b -up-Fe	0.253	0	-	-0.05	-	-
Center-up-Fe	(N)0.140	-	(Fe)0.317	-	-	-

Table 2. The average moment (Mom μ_B) and charge (Chg e) of four models. The charge of Fe_{II} in bulk Fe₄N is 7.61 $|e|$.

	Fe _{II} N-C		Fe _{II} N-NC		Fe _I Fe _{II} -C		Fe _I Fe _{II} -NC	
	Mom	Chg	Mom	Chg	Mom	Chg	Mom	Chg
	(μ_B)	(e)	(μ_B)	(e)	(μ_B)	(e)	(μ_B)	(e)
I-Fe _{II}	2.302	7.466	2.294	7.463	2.497	7.756	2.540	7.729
I-N(Fe _I)	-0.040	6.227	-0.048	6.211	2.905	7.896	2.835	7.896
II-Fe _{II}	1.514	7.684	1.268	7.730	2.049	7.656	2.078	7.660
II-N(Fe _I)	2.844	7.880	2.823	7.893	-0.016	6.246	-0.016	6.243
III-Fe _{II}	2.360	7.474	2.330	7.513	2.731	7.827	2.714	7.841
III-N(Fe _I)	-0.039	6.293	-0.043	6.214	3.011	7.905	3.006	7.890
C_t	-0.034	4.150	0.002	4.055	0.008	4.128	-0.018	4.199
C_b	-0.010	4.127	0.002	4.071	-0.009	4.188	-0.017	4.229
H	0.001	0.920	0.000	0.934	0.003	0.918	0.003	0.901
Center	-0.061	6.228	-	-	1.955	7.484	-	-
Fe_b	2.250	7.404	2.298	7.452	2.048	7.637	2.786	7.746
Fe_t	2.296	7.368	2.298	7.453	2.073	7.639	2.372	7.537

Figure captions

Figure 1. The structure of bulk Fe_4N and the side and top views of four benzene/ $\text{Fe}_4\text{N}(001)$ structures. The adsorption energies (E_{abs}) are labeled in Fig. 1(b).

Figure 2. The side and top views of charge density difference in four benzene/ $\text{Fe}_4\text{N}(001)$ structures. Yellow (blue) regions represent the net charge gain (loss).

Figure 3. The spin resolved density of states of the $\text{Fe}_{\text{II}}\text{N-C}$ and $\text{Fe}_{\text{II}}\text{N-NC}$ models.

Figure 4. The spin resolved density of states of the $\text{Fe}_{\text{I}}\text{Fe}_{\text{II}}\text{-C}$ and $\text{Fe}_{\text{I}}\text{Fe}_{\text{II}}\text{-NC}$ models.

Figure 5. Spin polarization nearby the benzene plane in the vacuum for these four models. (a) and (b) represent spin polarization distribution in $[E_F-0.4 \text{ eV}, E_F]$ energy interval; (c) and (d) represent spin-polarization distribution in $[E_F, E_F+0.4 \text{ eV}]$ energy interval. (a)/(d) is line profiles of the spin-polarization selected in (b)/(c), for different structures, respectively. The height of the spin-polarization distribution plane relative to the benzene plane are labeled

under (b) for each model.

Figure 6. The spin-resolved density of states of benzene adsorbed on $\text{Fe}_I\text{Fe}_{II}$ surface in the $E_F-1 \sim E_F+1$ eV interval.

Figure 7. The spin-polarization distribution vertical to Fe_4N surface for the $\text{Fe}_{II}\text{N-C}$ structure. This plane is parallel to $\text{Fe}_4\text{N}(100)$ and across the top site. The C_t atom is labeled and the value of ε is $E_F-0.4$ eV.

Figure 1, Q. Zhang *et al.*

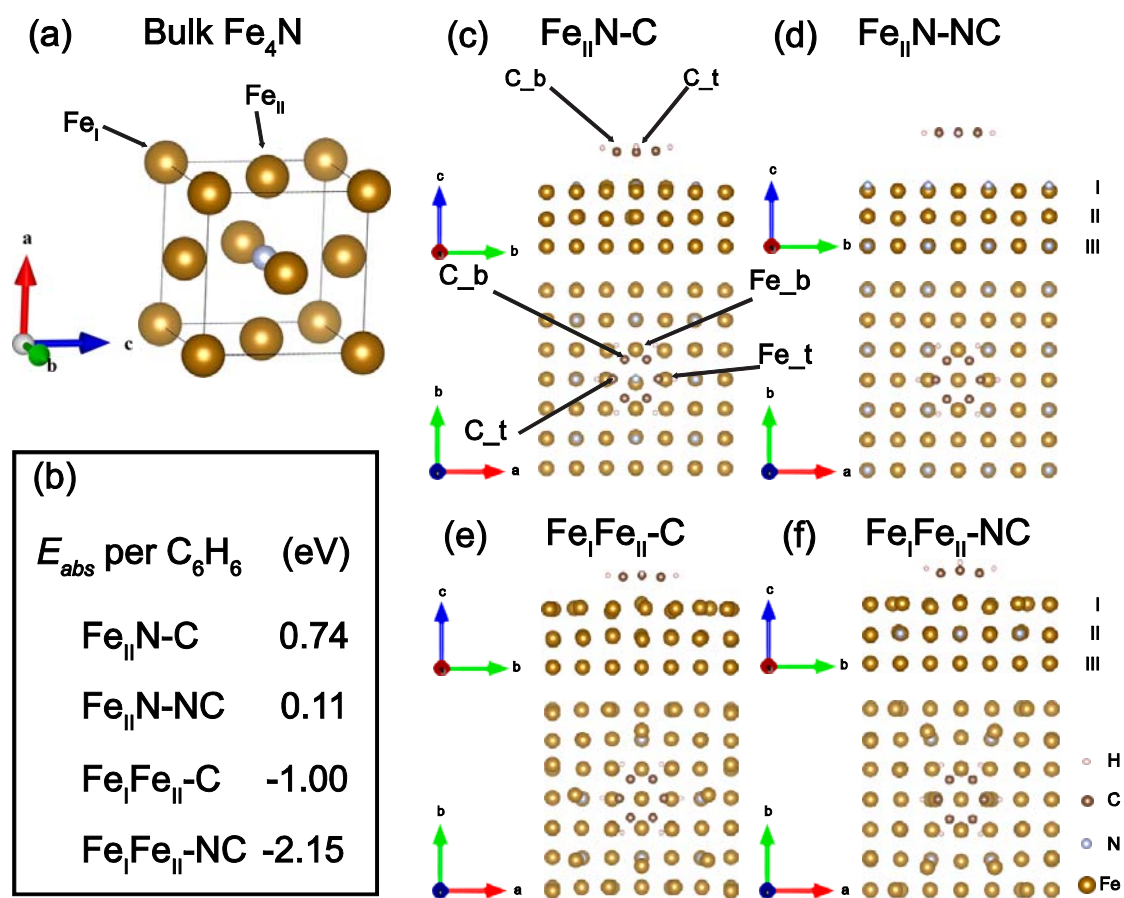


Figure 2, Q. Zhang *et al.*

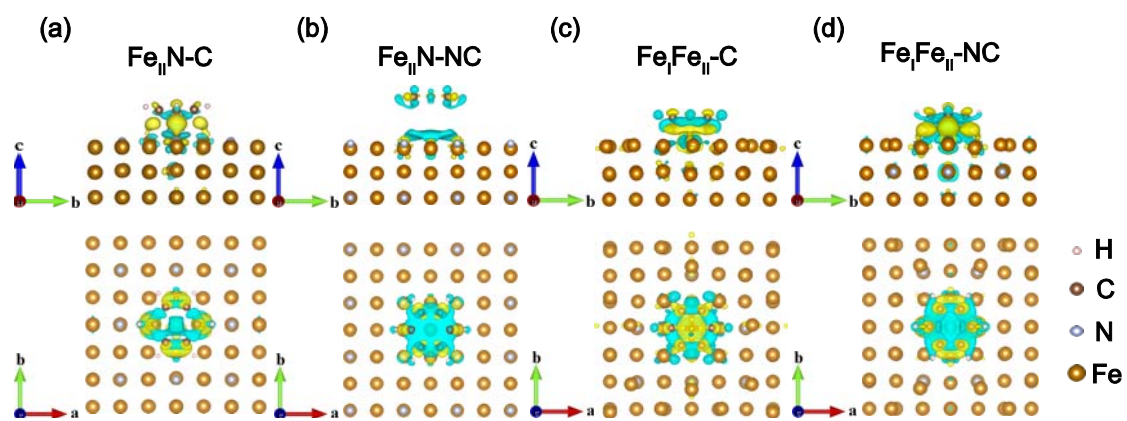


Figure 3, Q. Zhang *et al.*

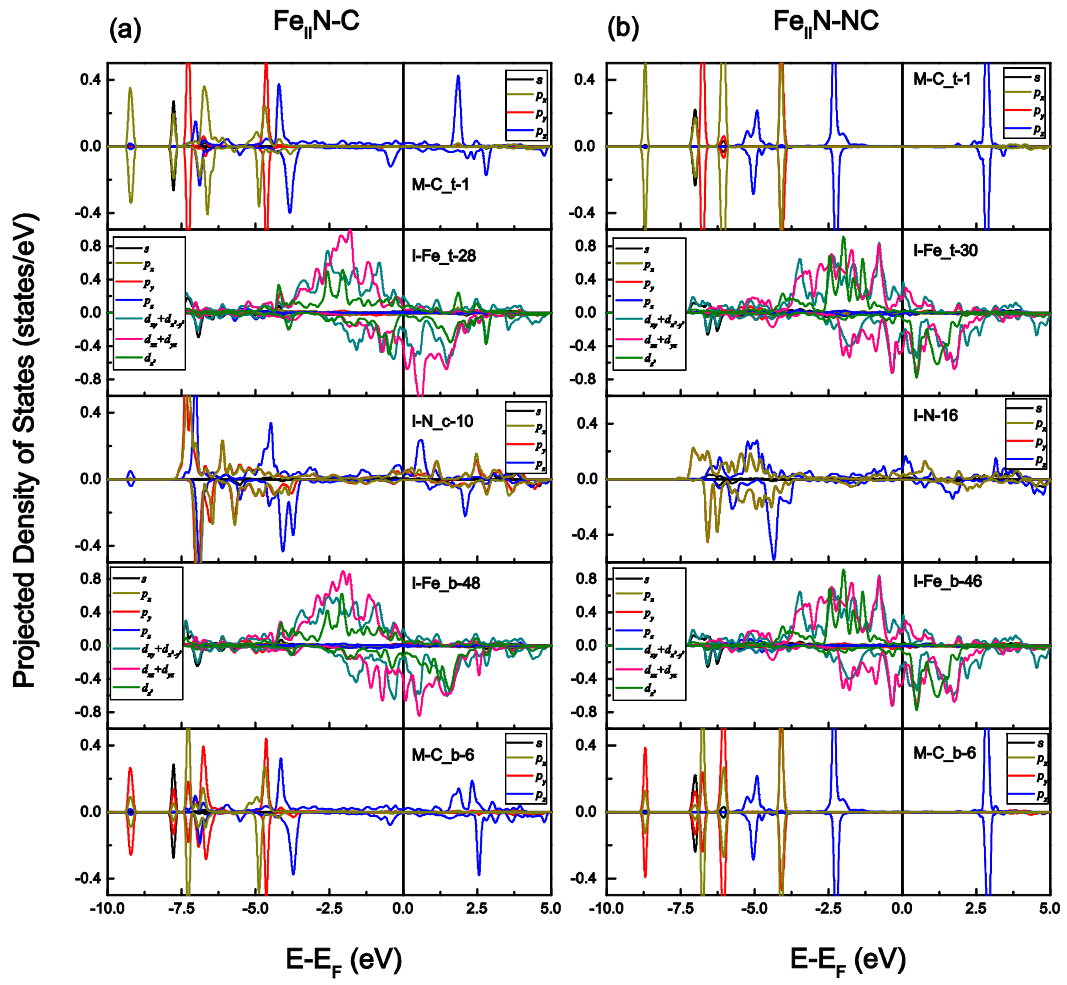


Figure 4, Q. Zhang *et al.*

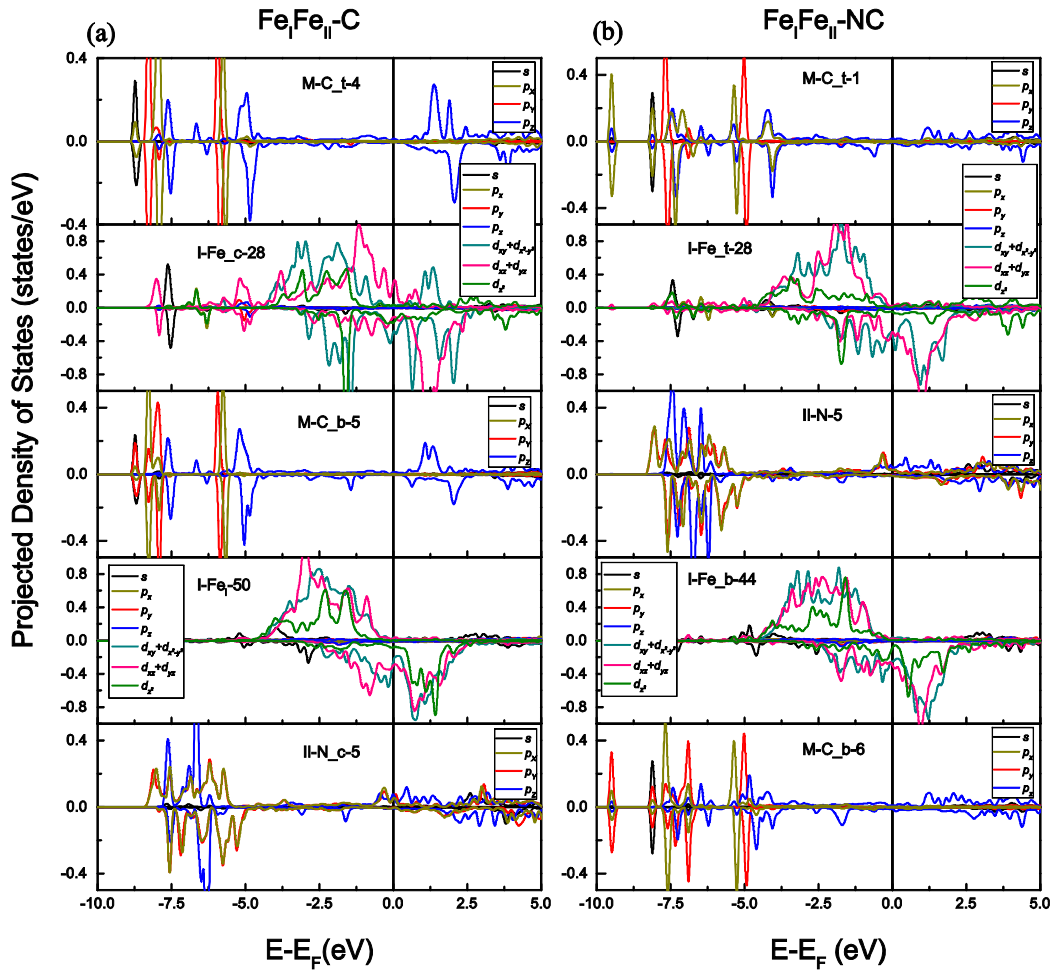


Figure 5, Q. Zhang *et al.*

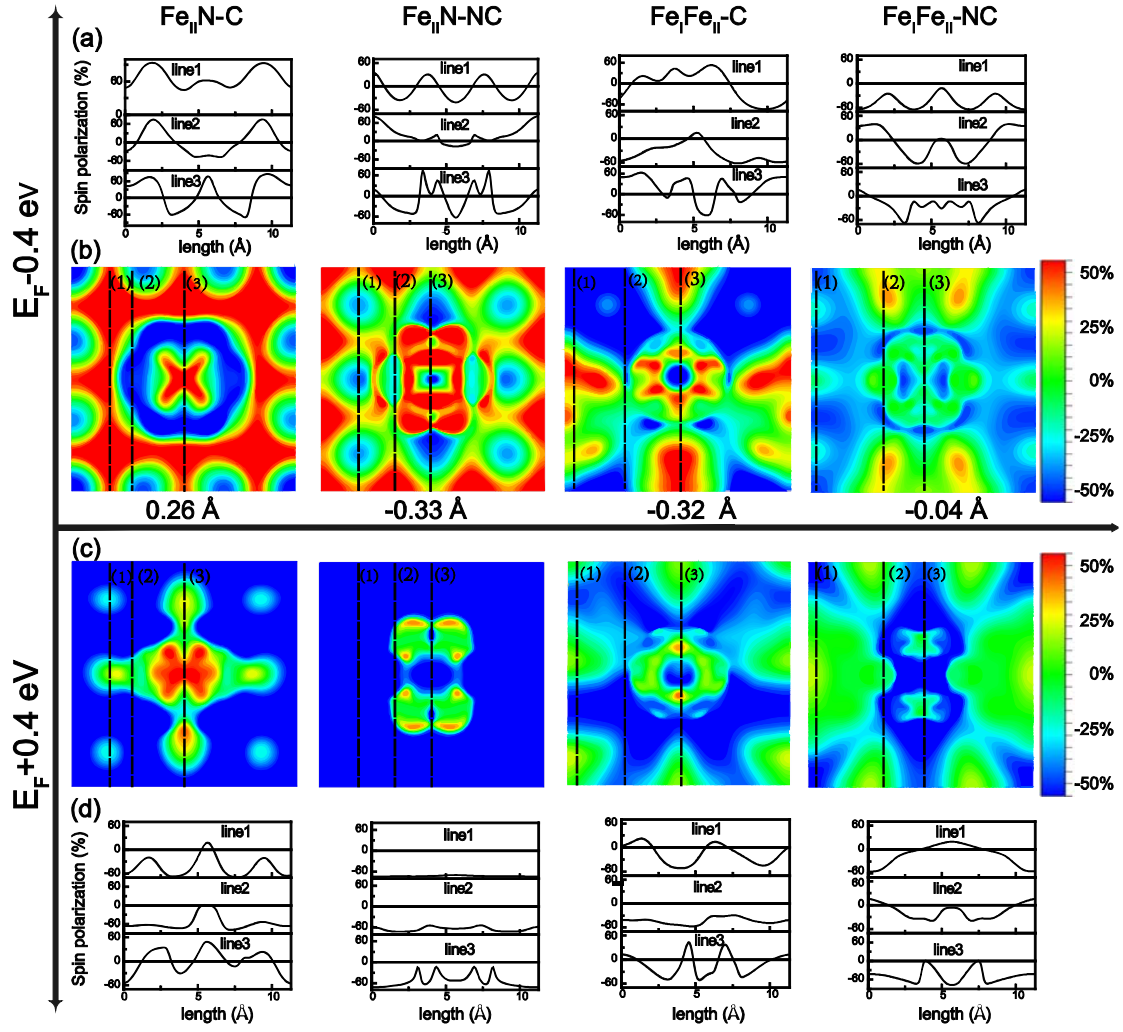


Figure 6, Q. Zhang *et al.*

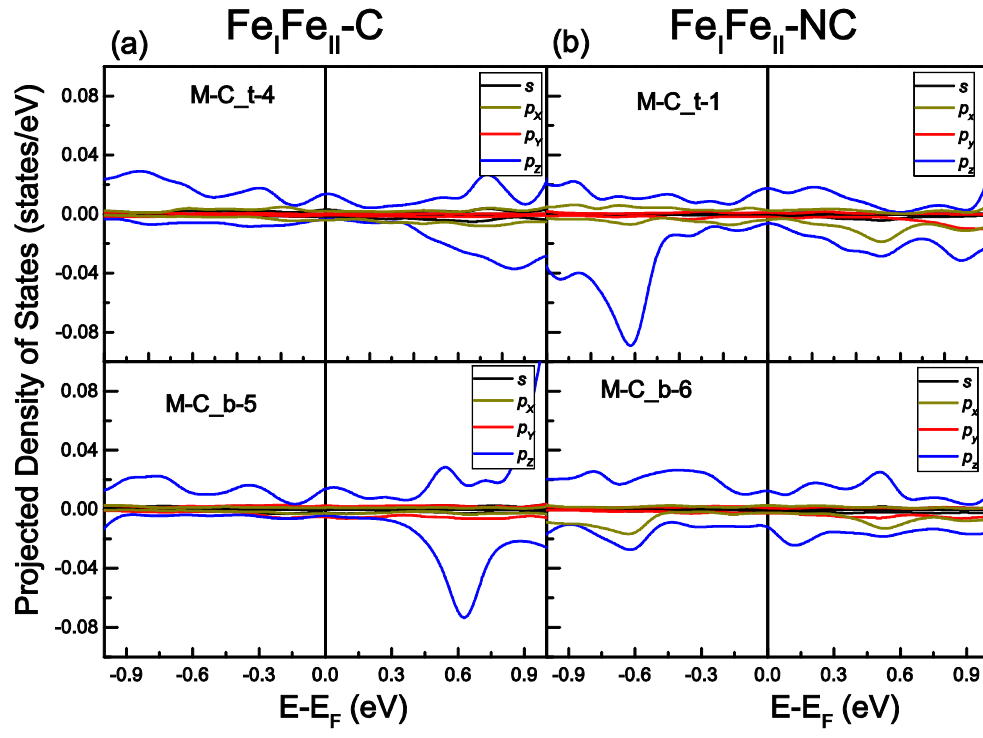


Figure 7, Q. Zhang *et al.*

